Electronic Supplementary Information

Coordinated single-molecule micelles: a self-template approach for preparing mesoporous doped carbons

Huijun Ouyang, Chenhong Fang, Zhi Xu, Le Li and Guyu Xiao[*]

Shanghai Key Laboratory of Electrical Insulation and Thermal Ageing, School of Chemistry and Chemical Engineering, State Key Laboratory of Metal Matrix Composites, Shanghai Jiao Tong University, Shanghai 200240

[*]*E-mail: gyxiao@sjtu.edu.cn*

1. Experimental Section

Materials

4-vinyl pyridine (4VP), styrene (St), CuCl, 4,4-bipyridine (bpy), (1-chloroethyl) benzene (1-PECl), tris(2-dimethylaminoethyl) amine (Me$_6$TREN), and zinc nitrate hexahydrate (Zn(NO$_3$)$_2$·6H$_2$O) were purchased from Adamas. 2-propanol, butane, *N,N*-dimethylformamide (DMF), dichloromethane (DCM), and petroleum ether (PE) were bought from Sigma Aldrich. 4VP and St were purified by the basic alumina column separation before polymerization. CuCl was purified by stirring in glacial acetic acid, followed by washing with ethanol and acetone three times. Other chemicals are of analytical grade and used as received.

Synthesis of macromolecular initiator

The macromolecular initiator was synthesized according to the literature.[1] The atom transfer radical polymerization (ATRP) was used to synthesize the macromolecular initiator. The solvent was the mixture of butane and 2-propanol, in which the volume ratio of butane to 2-propanol is 7:3. Typically, 3 mL of the mixed solvents, 409 mg of 4,4-bipyridine, 116 μL of 1-PECl, and 86.4 mg of CuCl were successively added in the Schlenk flask. The flask was fully degassed with three freeze-pump-thaw cycles and sealed under vacuum. Then, the flask was heated in an oil bath at 130 °C under stirring for ~5 h. After that, the resulting mixtures were dissolved in an appropriate amount of CH$_2$Cl$_2$, purified by neutral alumina-column separation, and then precipitated into excess methanol. After three times of precipitation-filtration and vacuum-drying at 40 °C for 24 h, the macromolecular initiator of the polystyrene

containing chloromethyl group (PS-Cl) was obtained. Its number-average molecular weight (M_n) and polydispersion index ($Đ$) are measured by gel permeation chromatography (GPC), which are 7,800 g mol^{-1} and 1.3, respectively.

Synthesis of polystyrene-*b*-poly(4-vinyl pyridine) (PS-*b*-P4VP)

The polymerization procedure is similar to the previous report.[1] In a typical process, 6 mL of the mixed solvents, 2.3 mg of PS-Cl, 80.2 μL of Me$_6$TREN, and 29.7 mg of CuCl were added in the Schlenk flask. After degassing, the flask was sealed and set in a water bath of 45 °C for 4 h. The product was precipitated in dichloromethane-petroleum ether and was dried in a vacuum oven at 40 °C for 24 h. The M_n and polydispersion index ($Đ$) of PS-*b*-P4VP are 13,500 g mol^{-1} and 1.2, respectively.

Preparation of the PS-*b*-P4VP micelles

PS-*b*-P4VP (1.0 g) was dissolved in 50 mL of DMF, which was stirred for 30 min to form a transparent solution. Subsequently, a milky solution appeared by adding deionized water to the polymer solution dropwise. Finally, the milky solution was poured into a dialysis tube and dialyzed with deionized water for several days to remove DMF. The concentration of the micelles was fixed to 5 mg mL^{-1}.

Preparation of the coordinated PS-*b*-P4VP micelles (CPMs)

4.6 mL of zinc nitrate solution (10 mg mL^{-1}) was poured into a 25 mL single-neck flask. Then, 5 mL of the as-prepared micelles was added dropwise under slow stirring. The mixtures were kept stirring for 24 h at room temperature, followed by freeze-drying for 2 days, forming the coordinated PS-*b*-P4VP micelle powders.

Preparation of the nitrogen-doped hierarchically porous carbons (NHPCs)

The as-synthesized PS-*b*-P4VP micelles were dried and annealed under N$_2$ at 400 °C for 2 h, and then further pyrolyzed under N$_2$ at 900 °C for another 2 h with a ramp rate of 2 °C min^{-1}. Subsequently, it was participated in 2 M HCl, followed by washing with water and drying in a vacuum oven to prepare the nitrogen-doped hierarchically porous carbons (NHPCs).

Structure Characterization

The gel permeation chromatography (GPC) was performed using tetrahydrofuran as the eluent on a Shimadzu Prominence System with a refractive index detector. A Bruker D8 advanced polyfunctional X-Ray diffractometer with Cu Kα (λ = 1.5418 Å) radiation was used to perform X-ray diffraction (XRD) measurement. Raman spectra were collected with an excitation wavelength of 532 nm using an Ar ion laser beam on a Senterra R200-L micro-Raman spectrometer. Scanning electron microscopy (SEM) was carried out on a JEOL JSM-7800F Prime apparatus and the SEM images were recorded using a 120 kV Tecnai G2 SpiritBiotwin electron microscope system. At 200 kV, the element mapping measurements were performed on a Talos F200X instrument. At 77 K, nitrogen adsorption/desorption isotherms were measured using an Autosorb-iQA3200-4 sorption analyzer. On an AXIS Ultra DLD system with an Al Kα achromatic X-ray source, an X-ray photoelectron spectroscopy (XPS) study was implemented, using a Vario EL cube for elemental analysis.

Electrochemical measurements

Glassy carbon rotating disk electrode (RDE) or rotating ring disk electrode (RRDE) was employed as the working electrode, while Ag/AgCl electrode and Pt wire are utilized as reference electrode and counter electrode in the electrochemical testings using a CHI760E electrochemical workstation, respectively. 4 mg of catalyst was dispersed in 490 uL ethanol and 10 uL 5 wt% Nafion under ultrasonication to make a well-dispersed suspension for the working electrode. The as-made carbon catalysts are used at a loading of 0.6 mg cm^{-2}. The 20% Pt/C catalyst is employed as a reference catalyst. The loading of Pt/C is 0.1 mg cm^{-2}. The RDE/RRDE tests were carried out in an O_2-saturated 0.1 M KOH solution with a rotation speed of 1600 rpm using linear sweep voltammetry (LSV) at a scan rate of 10 mV s^{-1} in the potential window of 0–1.2 V (vs. RHE). The LSV was performed at various rotating speeds (400, 900, 1600, and 2500 rpm) using a 10 mV s^{-1} sweep rate to determine the electron transfer number (n). The Koutecky-Levich equations can be used to calculate the electron transfer number (n):[2]

$$\frac{1}{J} = \frac{1}{J_L} + \frac{1}{J_K} = \frac{1}{B\omega^{1/2}} + \frac{1}{J_K}$$

$$B = 0.62nFC_0(D_0)^{2/3}v^{-1/6}$$

where J is the current density, J_L is the diffusion limiting current density, J_K is the kinetic current density, ω is the angular velocity of the disk, n is the electron transfer number, F is the Faraday constant (96,485 C mol^{-1}), C_0 is the bulk concentration of O_2 (1.2×10^{-6} mol cm^{-3}), D_0 is the diffusion coefficient of O_2 in 0.1 M KOH electrolyte (1.9×10^{-5} cm^2 s^{-1}), and v is the kinematics viscosity of electrolyte (0.01 cm^2 s^{-1}).

The cycling tests between 0.6 and 1.0 V at 200 mV s^{-1} in O_2-saturated 0.1 M KOH electrolyte were performed, and two LSV curves were recorded before and after continuous 5,000 cyclic voltammetry (CV) scanning from 0 to 1.2 V at a scan rate of 10 mV s^{-1} and a rotation speed rate of 1600 rpm. The methanol tolerance was tested at 0.6 V (RHE) and a rotating speed of 1600 rpm in O_2-saturated 0.1 M KOH by adding 10 mL methanol at the 300th second.

The electron transfer number (n) and hydrogen peroxide yield were investigated using RRDE tests. They were carried out from 0 to 1.2 V at a scan rate of 10 mV s^{-1} and a rotation speed rate of 1600 rpm in O_2-saturated 0.1 M KOH solution, setting the Pt ring voltage of 0.5 V. The following equations were used to calculate the electron transfer number (n) and H_2O_2 yield:[2]

$$n = 4 \times \frac{i_d}{i_r/N + i_d}$$

$$H_2O_2 \ (\%) = 200 \times \frac{i_r/N}{i_r/N + i_d}$$

where i_d is the disk current, i_r is the ring current, and N is the collection efficiency of the ring current ($N = 0.4$).

The electrochemical active surface area (ECSA) of the catalysts is calculated by the electrochemical double-layer capacitance (C_{dl}). The ECSA is measured on the RDE working electrode, which is calculated by the double-layer charging from the CV curves at various scan rates in non-Faradaic potential regions. The potential range is 1.05–1.15 V (vs. RHE). The scan rates are 2, 4, 6, 8, 10, and 12 mV s^{-1}, respectively. There is a linear relationship between the charging current and scan rate, and the correponding slope is C_{dl}.[28] The C_{dl} and ECSA obey the following equation of ECSA = $(C_{dl}/C_s)A_{geo}$, where C_s (0.04 mF cm^{-2}) and A_{geo} (0.07 cm^2) is the specific capacitance and geometric area of the glassy-carbon electrode, respectively.[3]

Assembly of the Zn-air batteries

The catalyst deposited on a gas diffusion layer was typically used as an air-cathode electrode (at a loading of 1 mg cm^{-2}), the anode electrode is Zn foil, and the electrolyte was 6 M KOH solution containing 0.2 M $ZnCl_2$.[4]

2. Figures and Tables
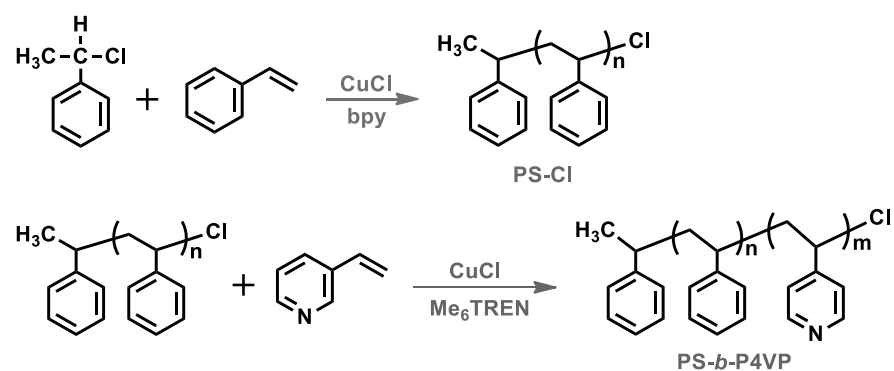
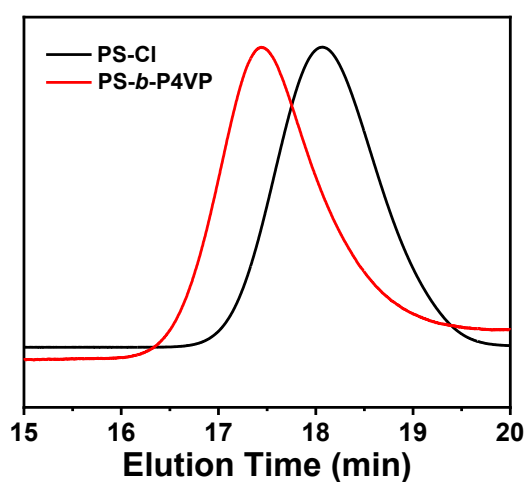**Scheme S1.** Synthetic routes of PS-Cl and PS-*b*-P4VP.

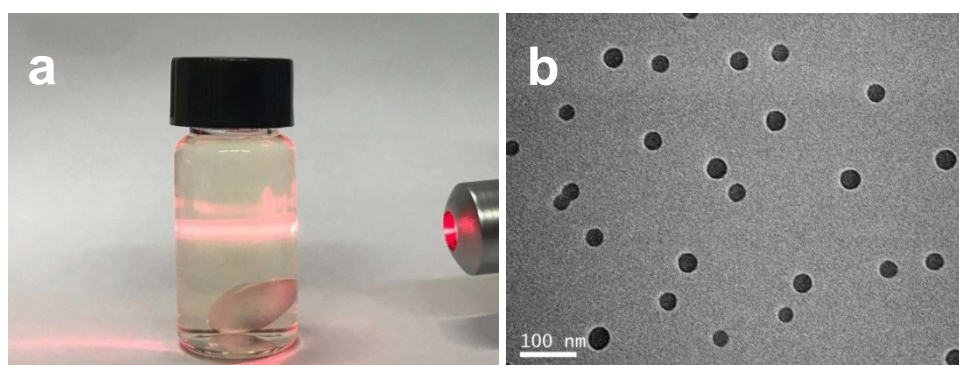**Figure S1.** GPC curves of PS-Cl and PS-*b*-P4VP.

Figure S2. (a) Tyndall phenomenon of the PS-*b*-P4VP colloids, (b) TEM image of the PS-*b*-P4VP micelles.
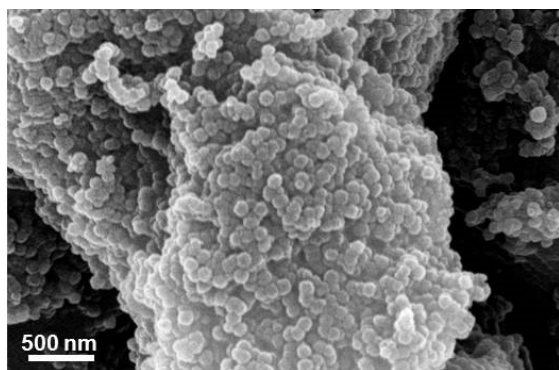
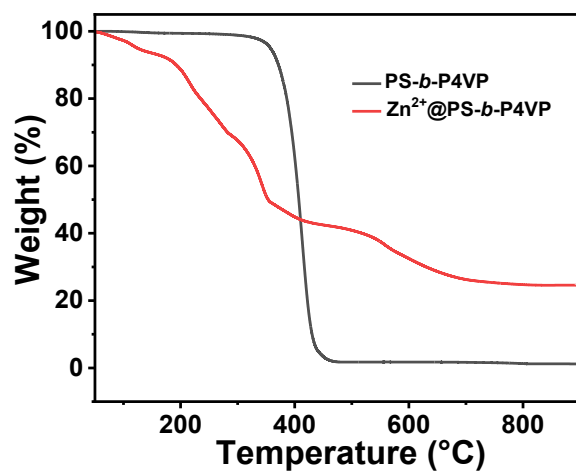**Figure S3.** SEM image of the CPM aggregations.

Figure S4. TGA curves of PS-*b*-P4VP and the Zn^{2+}-coordinated PS-*b*-P4VP micelles (CPMs).
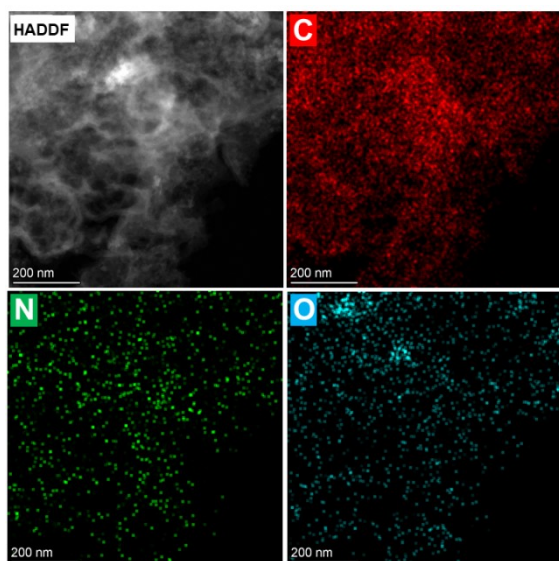

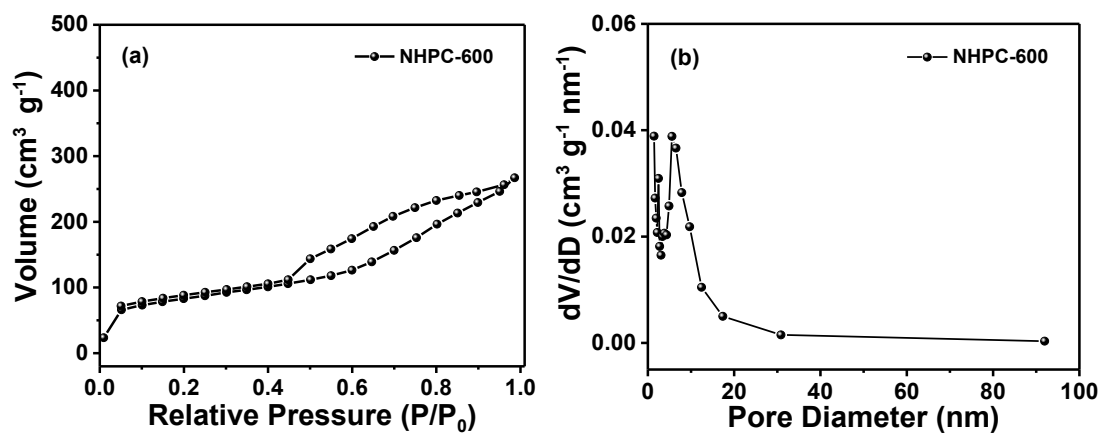**Figure S5.** HADDF image and the corresponding element mappings of NHPC-900.

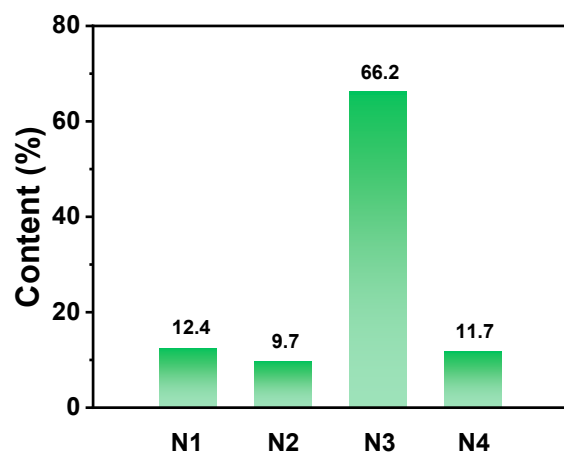**Figure S6.** (a) N_2 adsorption/desorption isotherms and (b) pore-diameter distribution curve of NHPC-600.

Figure S7. Percentage histogram of the pyridine N (N_1), pyrrolic N (N_2), graphitic N (N_3), and oxidic N (N_4) in NHPC-900.
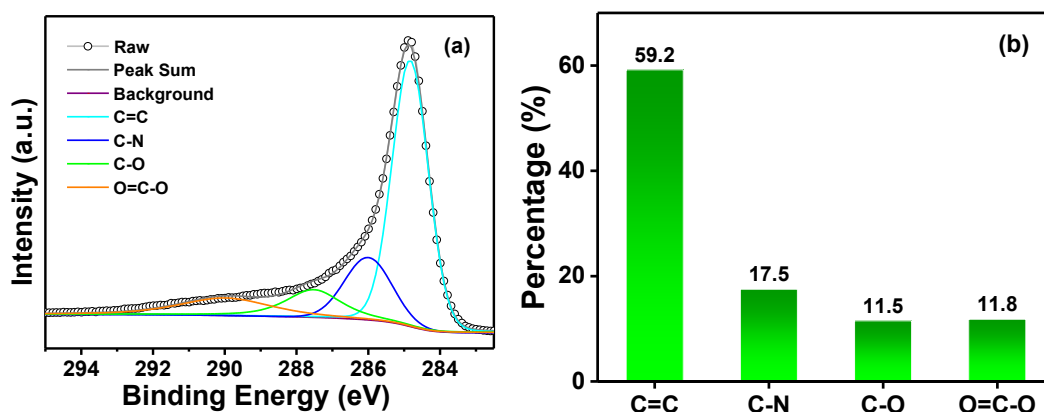

Figure S8. (a) High-resolution C 1s XPS spectrum of NHPC-900 and (b) its percentage histogram of various C-containing groups.
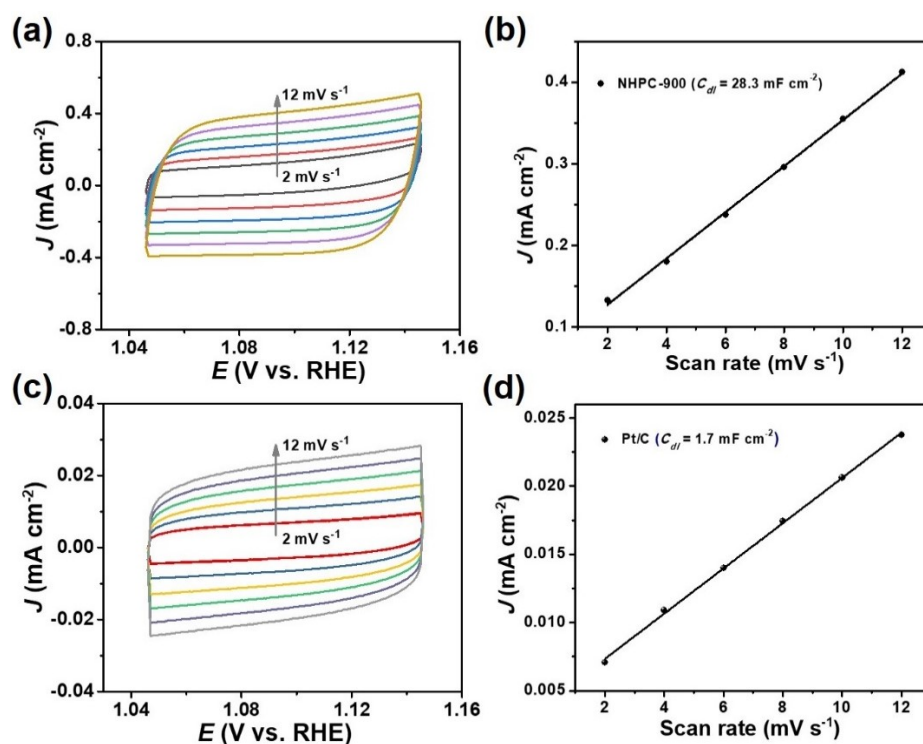
Figure S9. (a, c) CV curves of NHPC-900 and Pt/C in non-Faradaic potential range at various scan rates in 0.1 M KOH; (b, d) Capacitive current derived from CV curves at 1.10 V as a function of scan rate.
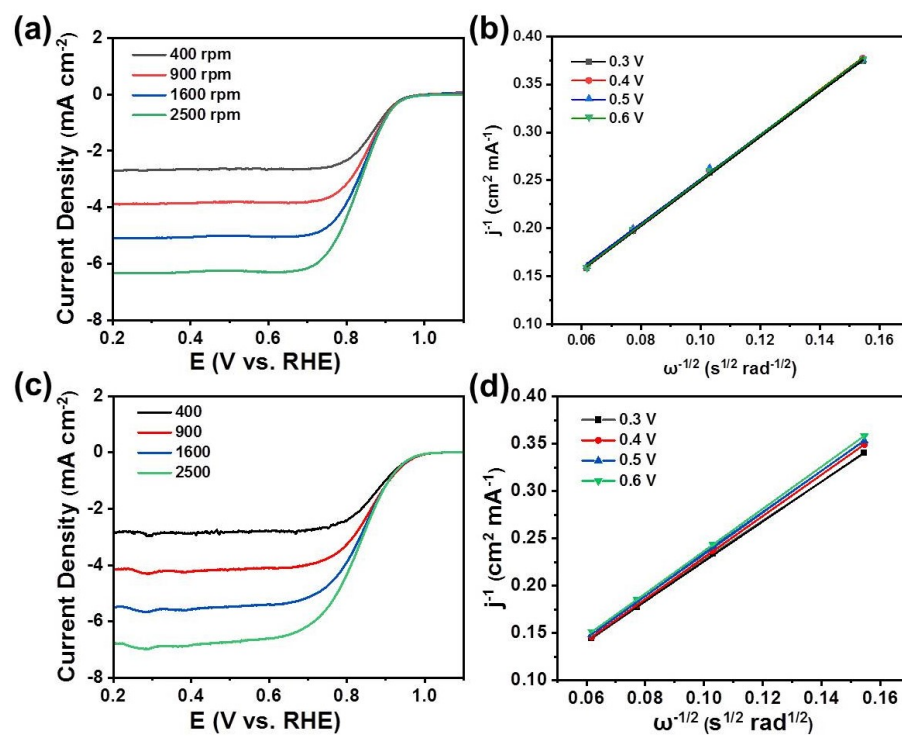

Figure S10. LSV curves at various rotating rates (*left*) and Koutecky-Levich plots (*right*): (a, b) NHPC-900, (c, d) Pt/C.
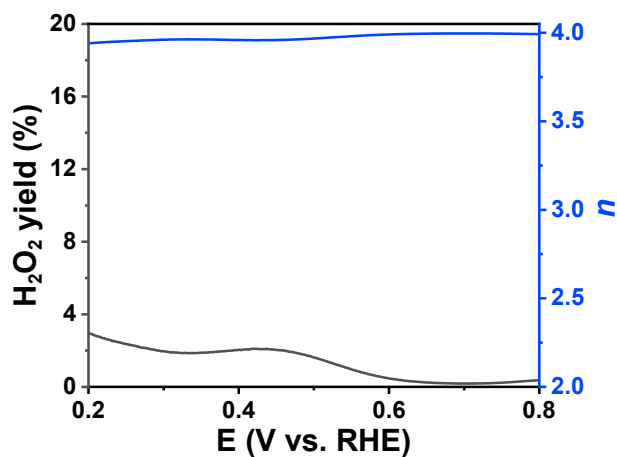
Figure S11. H_2O_2 yield and electron transfer number (*n*) of Pt/C determined by the RRDE testings.
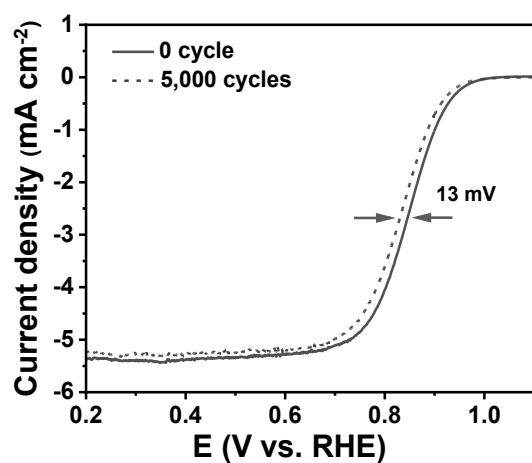

Figure S12. LSV curves of Pt/C before and after 5,000 cycles in O_2-saturated 0.1 M KOH.
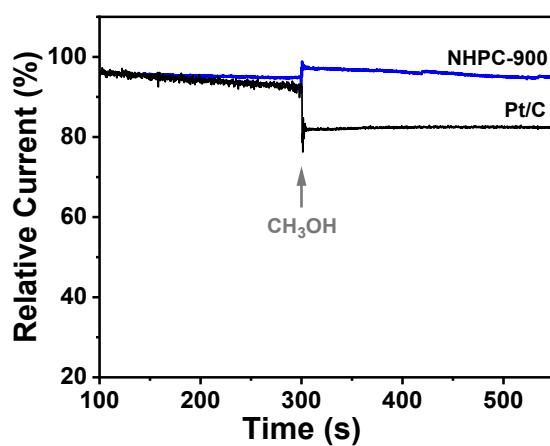

Figure S13. Current-time (*i–t*) chronoamperometric response of NHPC-900 and Pt/C in O_2-saturated 0.1 M KOH before and after adding 1 M CH_3OH at the 300th second.
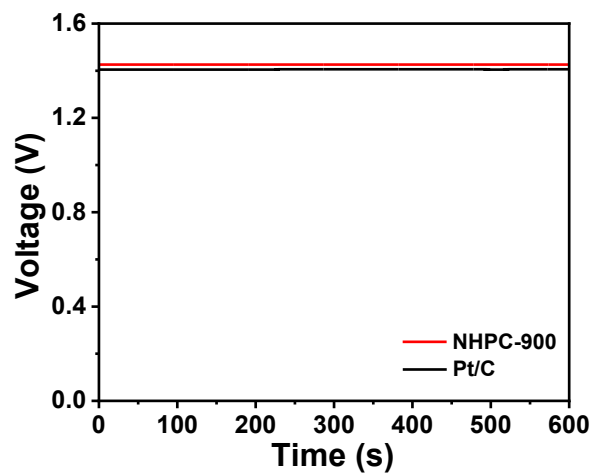
Figure S14. Open circuit potential of NHPC-900 and Pt/C.

Table S1. Pore-structure parameters of NHPC-900 and -600.

Samples	S_{BET}^a (m^2 g^{-1})	S_{mic}^b (m^2 g^{-1})	V_{total}^c (cm^3 g^{-1})	V_{micro}^d (cm^{-3} g^{-1})	D_{BJH}^e (nm)
NHPC-900	1168	626	1.16	0.30	9.0
NHPC-600	250	132	0.39	0.05	7.0

^{a} specific surface area calculated from the N$_2$ adsorption-desorption isotherms, ^{b} specific surface area of micropores calculated by the V–T plot, ^{c} total pore volume, ^{d} pore volume of micropores calculated by the V–T plot, ^{e} average pore-diameter calculated from the pore-size distribution curves using the BJH method.

Table S2. Element contents of NHPC-900 measured by XPS.

Elements	Position (eV)	Percentage at.%	Percentage wt%
C 1s	284.89	91.68	89.47
O 1s	533.29	6.61	8.59
N 1s	401.09	1.71	1.94

Table S3. ORR catalytic performances of NHPC-900 and highly efficient metal-free doped carbons in 0.1 M KOH.

Catalysts	E_{onset} V (RHE)	$E_{1/2}$ V (RHE)	J_L (mA cm^{-2})	Reference
Carbon plates	0.94	0.835	5.36	*Adv. Mater.* 2018, 30, 1803588 [5]
B,N-doped carbon	0.98	0.84	~5.5	*Adv. Sci.* 2018, 5, 1800036 [6]
N-GNR@CNT	0.99	0.84	5.1	*Nat. Commun.* 2018, 9, 3819 [7]
Modified fullerene	0.911	0.833	5.29	*Angew. Chem. Int. Ed.* 2019, 58, 3859 [8]
M-PNC	0.95	0.84	5.3	*Chem. Sci.* 2020, 11, 9584 [9]
SCNS	0.85	0.770	5.05	*Angew. Chem. Int. Ed.* 2020, 59, 19627 [10]
Pt/C	0.944	0.84	5.5	This work
NHPC-900	**0.968**	**0.85**	**5.5**	**This work**

Table S4. Performances of the Zn-air batteries with NHPC-900 and highly efficient metal-free doped carbons as air-cathode catalysts.

Catalysts	Loading (mg cm^{-2})	Cell voltage (V)	PPD[*] (mW cm^{-2})	Specific capacity (mAh g^{-1})	Energy Density (Wh kg^{-1})	Ref.
NDGs-800	1.0	1.23 (@10 mA cm^{-2})	115.2	750.8 (@10 mA cm^{-2})	872.3 (@10 mA cm^{-2})	[4]
Si-N-C-6	0.9	1.24 (@20 mA cm^{-2})	100	800 (@20 mA cm^{-2})	990 (@20 mA cm^{-2})	[11]
NPCS-900	1.5	1.23 (@2 mA cm^{-2})	79	684(@2 mA cm^{-2}) 625(@2 mA cm^{-2})	848(@2 mA cm^{-2}) 656(@20 mA cm^{-2})	[12]
NSC-1000	2.0	1.24 (@10 mA cm^{-2})	167.8	634 (@100 mA cm^{-2})	581 (@100 mA cm^{-2})	[13]
CC-3	0.05	1.18 (@10 mA cm^{-2})	85	714 (@10 mA cm^{-2})	/	[14]
GPCNSs	2	1.28 (@10 mA cm^{-2})	128	756 (@10 mA cm^{-2})	/	[15]
Pt/C	1.0	1.24 (10 mA cm^{-2})	127	779 (@10 mA cm^{-2})	934 (@10 mA cm^{-2})	This work
NHPC-900	**1.0**	**1.29 (10 mA cm^{-2})**	**173**	**775 (@10 mA cm^{-2})**	**965 (@10 mA cm^{-2})**	**This work**

[*] Peak power density

REFERENCES

1. N.V. Tsarevsky, W.A. Braunecker, S.J. Brooks, K. Matyjaszewski, *Macromolecules*, 2006, **39**, 6817–6824.

2. X. Peng, L. Zhang, Z. Chen, L. Zhong, D. Zhao, X. Chi, X. Zhao, L. Li, X. Lu, K. Leng, C. Liu, W. Liu, W. Tang, K.P. Loh, *Adv. Mater.*, 2019, **31**, 1900341.

3. Y. Wu, X. Li, Y. Wei, Z. Fu, W. Wei, X. Wu, Q. Zhu and Q. Xu, *Adv. Mater.*, 2021, **33**, 2006965.

4. Q. Wang, Y. Ji, Y. Lei, Y. Wang, Y. Wang, Y. Li and S. Wang, *ACS Energy Lett.*, 2018, **3**, 1183–1191.

5. J. Han, G. Huang, Z. Wang, Z. Lu, J. Du, H. Kashani and M. Chen, *Adv. Mater.*, 2018, **30**, 1803588.

6. T. Sun, J. Wang, C. Qiu, X. Ling, B. Tian, W. Chen and C. Su, *Adv. Sci.*, 2018, **5**, 1800036.

7. L. Xue, Y. Li, X. Liu, Q. Liu, J. Shang, H. Duan, L. Dai and J. Shui, *Nat. Commun.*, 2018, **9**, 3819–3826.

8. J. Zhu, Y. Huang, W. Mei, C. Zhao, C. Zhang, J. Zhang, I. S. Amiinu and S. Mu, *Angew. Chem. Int. Ed.*, 2019, **58**, 3859–3864.

9. W. Xia, M. A. Hunter, J. Wang, G. Zhu, S. J. Warren, Y. Zhao, Y. Bando, D. J. Searles, Y. Yamauchi and J. Tang, *Chem. Sci.*, 2020, **11**, 9584–9592.

10. L. Zou, C. C. Hou, Q. Wang, Y. S. Wei, Z. Liu, J. S. Qin, H. Pang and Q. Xu, *Angew. Chem. Int. Ed.*, 2020, **59**, 19627–19632.

11. Q. Wei, M. Cherif, G. Zhang, A. Almesrati, J. Chen, M. Wu, N. Komba, Y. Hu, T. Regier, T.-K. Sham, F. Vidal and S. Sun, *Nano Energy*, 2019, **62**, 700–708.

12. S. Chen, L. Zhao, J. Ma, Y. Wang, L. Dai and J. Zhang, *Nano Energy*, 2019, **60**, 536–544.

13. K. Yuan, C. Lu, S. Sfaelou, X. Liao, X. Zhuang, Y. Chen, U. Scherf and X. Feng, *Nano Energy*, 2019, **59**, 207–215.

14. C. Liu, F. Liu, H. Li, J. Chen, J. Fei, Z. Yu, Z. Yuan, C. Wang, H. Zheng, Z. Liu, M. Xu, G. Henkelman, L. Wei and Y. Chen, *ACS Nano*, 2021, **15**, 3309–3319.

15. Y. Chen, J. Huang, Z. Chen, C. Shi, H. Yang, Y. Tang, Z. Cen, S. Liu, R. Fu and D. Wu, *Adv. Sci.*, 2022, **9**, 2103477.